Signatures of Anomalous Transport in the 2019/2020 Arctic Stratospheric Polar Vortex

Gloria L Manney[1], Luis Millan[2], Michelle L. Santee[3], Krzysztof Wargan[4], Alyn Lambert[5], Jessica L. Neu[6], Frank Werner[3], Zachary Duane Lawrence[7], Michael J. Schwartz[8], Nathaniel J Livesey[3], and William G. Read[5]

[1]Northwest Research Associates
[2]Jet propulsion laboratory
[3]Jet Propulsion Laboratory
[4]Science Systems and Applications, Inc.
[5]Jet Propulsion Lab (NASA)
[6]Jet Propulsion Laboratory / Caltech
[7]CIRES/NOAA
[8]Jet Propulsion Laboratory, California Institute of Technology

November 23, 2022

Abstract

The exceptionally strong and long-lived Arctic stratospheric polar vortex in 2019/2020 resulted in large transport anomalies throughout the fall-winter-spring period from vortex development to breakup. These anomalies are studied using Aura MLS long-lived trace gas data for N_2O, H_2O,and CO, ACE-FTS CH_4 , and meteorological and trace gas fields from reanalyses. Strongest anomalies are seen throughout the winter in the lower through middle stratosphere (from about 500K through 700K), with record low (high) departures from climatology in N_2O and CH_4 (H_2O). CO also shows extreme high anomalies in midwinter through spring down to about 550K. Examination of descent rates, vortex confinement, and trace gas distributions in the preceding months indicates that the early-winter anomalies in N_2O and H_2O arose primarily from entrainment of air with already-anomalous values (which likely resulted from transport linked to an early January sudden stratospheric warming the previous winter during a favorable quasi-biennial oscillation phase) into the vortex as it developed in fall 2019 followed by descent of those anomalies to lower levels within the vortex. Trace gas anomalies in midwinter through the late vortex breakup in spring 2020 arose primarily from inhibition of mixing between vortex and extravortex air because of the exceptionally strong and persistent vortex. Persistent strong N_2O and H_2O gradients across the vortex edge demonstrate that air within the vortex and its remnants remained very strongly confined through late April (mid-May) in the middle (lower) stratosphere.

Signatures of Anomalous Transport in the 2019/2020 Arctic Stratospheric Polar Vortex

Gloria L. Manney[1,2], Luis F. Millán[3], Michelle L. Santee[3], Krzysztof Wargan[4,5], Alyn Lambert[3], Jessica L. Neu[3], Frank Werner[3], Zachary D. Lawrence[6,7], Michael J. Schwartz[3], Nathaniel J. Livesey[3], William G. Read[3]

[1]NorthWest Research Associates, Socorro, NM, USA
[2]New Mexico Institute of Mining and Technology, Socorro, NM, USA
[3]Jet Propulsion Laboratory, California Institute of Technology, Pasadena, CA, USA
[4]NASA Goddard Space Flight Center, Greenbelt, MD, USA
[5]Science Systems and Applications, Inc., Lanham, MD, USA
[6]Cooperative Institute for Research in Environmental Sciences (CIRES) & NOAA Physical Sciences Laboratory (PSL), University of Colorado, Boulder, Colorado, USA.
[7]NorthWest Research Associates, Boulder, CO, USA

Key Points:

- Anomalies in long-lived trace gases in the exceptionally strong 2019/2020 stratospheric polar vortex are studied using Aura MLS measurements
- Fall/early winter trace gas anomalies arose mainly from entrainment of existing anomalies into the developing vortex followed by descent
- Inhibition of mixing between air within and outside of the strong and persistent vortex led to midwinter/spring transport anomalies

Corresponding author: Gloria L Manney, `manney@nwra.com`

Abstract

The exceptionally strong and long-lived Arctic stratospheric polar vortex in 2019/2020 resulted in large transport anomalies throughout the fall-winter-spring period from vortex development to breakup. These anomalies are studied using Aura MLS long-lived trace gas data for N_2O, H_2O, and CO, ACE-FTS CH_4, and meteorological and trace gas fields from reanalyses. Strongest anomalies are seen throughout the winter in the lower through middle stratosphere (from about 500 K through 700 K), with record low (high) departures from climatology in N_2O and CH_4 (H_2O). CO also shows extreme high anomalies in midwinter through spring down to about 550 K. Examination of descent rates, vortex confinement, and trace gas distributions in the preceding months indicates that the early-winter anomalies in N_2O and H_2O arose primarily from entrainment of air with already-anomalous values (which likely resulted from transport linked to an early January sudden stratospheric warming the previous winter during a favorable quasi-biennial oscillation phase) into the vortex as it developed in fall 2019 followed by descent of those anomalies to lower levels within the vortex. Trace gas anomalies in midwinter through the late vortex breakup in spring 2020 arose primarily from inhibition of mixing between vortex and extravortex air because of the exceptionally strong and persistent vortex. Persistent strong N_2O and H_2O gradients across the vortex edge demonstrate that air within the vortex and its remnants remained very strongly confined through late April (mid-May) in the middle (lower) stratosphere.

Plain Language Summary

The wintertime Arctic stratospheric polar vortex in 2019/2020 was exceptionally strong and persisted unusually late into spring. This led to Arctic ozone loss and impacts on Northern Hemisphere weather. We use measurements of long-lived trace gases from two satellite instruments that have been observing for over 17 years to study how isolated the air inside the vortex was from that outside; the degree of mixing between interior and exterior air is controlled by the strength of the vortex. In 2019/2020, these gases, which are not affected by chemistry during the study period, showed the largest departures from typical values ever observed. We found that the anomalies arose from two sources: In fall and early winter, pre-existing extreme values were incorporated into the stratospheric polar vortex as it developed and then were transported downward to lower levels. In late winter and spring, the trace gas concentrations were unusual because air was almost completely confined within the exceptionally strong and persistent vortex and remained that way much longer than usual. These results have implications for the evolution of trace gases that can affect radiative processes related to climate.

1 Introduction

The stratospheric polar vortex in the 2019/2020 Arctic winter was the strongest, most persistent, and most consistently cold on record (e.g., Lawrence et al., 2020). Persistently low temperatures as well as vortex confinement later in spring than usual resulted in record low ozone in the lower stratospheric vortex (lower than that in 2010/2011, the previous record, e.g., Manney et al., 2020; Wohltmann et al., 2020, 2021; Weber et al., 2021). Such an exceptionally strong stratospheric polar vortex was associated with substantial changes in the middle atmospheric circulation extending through the stratosphere and above (e.g., Lawrence et al., 2020; Lukianova et al., 2021; Ma et al., 2022), as well as coupling with the troposphere (e.g., Lawrence et al., 2020; Rupp et al., 2022).

Strong and persistent vortex confinement such as that in 2019/2020 not only is critical to extended polar processing in the lower stratospheric vortex but is also associated with anomalies in 3D transport. Most obvious, perhaps, is the association of a stronger vortex with weak mixing across its edge. Furthermore, a more persistent vortex results in substantial confinement within it later into the spring (including confinement of low ozone resulting from chemical depletion) (Knudsen & Grooß, 2000; Marchand et al., 2003; Manney, Santee, et al., 2011; Manney & Lawrence, 2016; Manney et al., 2020, and references therein). Several studies focusing primarily on the exceptional ozone loss in 2019/2020 have noted in passing some aspects of anomalous transport;

in particular, Manney et al. (2020) reported atypically low N_2O in the lower stratospheric vortex seen in Aura Microwave Limb Sounder (MLS) data starting as early as November 2019. Unusually low N_2O could arise from stronger diabatic descent, descent of lower values, reduced mixing across the vortex edge, or a combination of these processes. Manney et al. (2020) also noted unusually high H_2O, which would be consistent with transport effects controlling both species' evolution. Using ground-based column HF measurements in the high Arctic as a tracer of vertical motion, Bognar et al. (2021) suggest that descent may have been weaker than usual in 2019/2020, but this result is uncertain because of the limited data in other years for comparison and because of the difficulty of distinguishing these effects in column data. Inness et al. (2020) and Feng et al. (2021) both show that dynamical and transport processes resulted in less replenishment of ozone in spring 2020 than is typical in the Arctic. Their analysis, primarily using column ozone, did not allow the effects of descent to be distinguished from those of mixing. In addition, they were unable to differentiate between transport-related effects (such as variations in descent and mixing) and the dynamical impact of large interannual variations in temperature on column ozone amounts via the density-induced correlation between temperature and column ozone. (See, e.g., supplementary information for Manney, Santee, et al. (2011, and references therein) for discussion of the difficulty in distinguishing dynamical and transport effects using column ozone measurements and the dynamical relationship of low temperatures to low column ozone.) The 3D structure of trace gas profiles, differences in which can also result in anomalies in the absence of anomalous descent or mixing rates, have not been explored. Thus, while some evidence of anomalies in transport has been presented, the relationships between various dynamical / transport processes and 3D trace gas evolution that lead to those anomalies is as yet unclear.

Another aspect of transport was discussed by Curbelo et al. (2021), who used Lagrangian methods along with tagging parcels with MLS ozone values inside the vortex. They described an event during which the vortex split in two in the lower to middle stratosphere in late April. Lagrangian transport calculations showed that while the smaller vortex remnant decayed, the larger vortex persisted for several more weeks in the lower stratosphere, confining air with depleted ozone until the final vortex breakup. That paper provides an example of how the details of transport within the vortex during one brief event were instrumental in determining aspects of ozone loss and the role of transport effects (e.g., dispersal from the vortex or lack thereof) in determining the fate of ozone-depleted vortex air.

Beyond these indications of anomalies, transport throughout the polar stratosphere during the 2019/2020 winter has not to our knowledge previously reported in detail. The long-lived trace gases N_2O, H_2O, and CO measured by MLS (along with O_3 in the upper troposphere / lower stratosphere, UTLS) provide a suite of observations well-suited to this task, and these observations have been used in numerous previous studies of transport in the polar middle atmosphere (e.g., Manney, Harwood, et al., 2009; Manney, Schwartz, et al., 2009; Manney, Lawrence, Santee, Read, et al., 2015; Lee et al., 2011; McDonald & Smith, 2013; Tao et al., 2015; Harvey et al., 2018; Wargan et al., 2020). In this paper, we use these data, augmented by observations of CH_4 from the Atmospheric Chemistry Experiment-Fourier Transform Spectrometer (ACE-FTS) and by meteorological and chemical reanalysis data, to provide a broad overview of the striking anomalies in transport in and around the exceptional stratospheric polar vortex in 2019/2020.

2 Data and Analysis

2.1 MERRA-2 Data and Derived Products

The Modern Era Retrospective analysis for Research and Applications, Version 2 (MERRA-2) (Gelaro et al., 2017) produced by NASA's Global Modeling and Assimilation Office is one of the current generation of reanalyses that provide meteorological data from comprehensive data assimilation systems at relatively high resolution. MERRA-2 uses 3D-Var assimilation with Incremental Analysis Update (IAU) (Bloom et al., 1996) to constrain the analyses. The MERRA-2 data products used here are provided every three hours on model levels and a $0.5^\circ \times 0.625^\circ$ latitude/longitude grid (near the resolution of the "cubed-sphere" grid of the underlying atmospheric model). The MERRA-2 vertical grid ranges from about 0.8 km spacing in the upper troposphere to about 1.8 km near the stratopause. The MERRA-2 "Assimilated" data collection (Global Modeling and Assimilation Office (GMAO), 2015) used here is recommended by GMAO for most studies, especially those involving transport (Global Modeling and Assimilation Office (GMAO), 2017). MERRA-2 is one of several modern reanalyses that have been demonstrated to be suitable for polar processing and stratospheric transport studies via intercomparisons of processes including mixing and horizontal and vertical transport (Fujiwara et al., 2022, see especially Chapters 5, 6, and 10, and references therein).

Meteorological information is derived from MERRA-2 as described by Manney et al. (2007); Manney, Hegglin, et al. (2011), typically either interpolated to or derived at all satellite measurement locations and times. These fields are used not only for meteorological context, but also to produce vortex-averaged and equivalent latitude / potential temperature coordinate mappings of the satellite data as described below.

2.2 Satellite Data

Aura MLS (Waters et al., 2006) measures thermal emission of the atmosphere from the upper troposphere into the mesosphere. The instrument, operating since mid-2004, makes day and night measurements between 82°S and 82°N along 15 orbits per day. Here we use version 5 MLS N_2O, H_2O, CO, and O_3 (Lambert, Livesey, & Read, 2020; Lambert, Read, & Livesey, 2020; Schwartz, Pumphrey, et al., 2020; Schwartz, Froidevaux, et al., 2020; Livesey et al., 2020) from the 2004/2005 through 2019/2020 Arctic winters to reveal signatures of the anomalous transport in 2019/2020. Recommended quality screening (Livesey et al., 2020) is applied to all MLS observations prior to further processing. The products used herein, comprising vortex-averaged and equivalent latitude / potential temperature mapped fields, are from the publicly available "Level 3" (L3) MLS datasets (Lambert et al., 2021b, 2021a; Schwartz, Pumphrey, et al., 2021; Schwartz, Froidevaux, et al., 2021; Livesey et al., 2020).

ACE-FTS, on Canada's SCISAT-1 satellite (Bernath et al., 2005), is a solar occultation sensor that makes sunrise and sunset measurements of many species, providing up to 30 high-resolution profiles per day, in an orbit optimized to highlight the polar regions in winter. In addition to showing consistency of ACE-FTS N_2O, H_2O and CO data with those from MLS, we augment the long-lived tracer measurements used here with ACE-FTS CH_4. We use version 4.1 ACE-FTS retrievals (Boone et al., 2020), quality-screened using flags provided by the instrument team (P. E. Sheese et al., 2015; P. Sheese & Walker, 2020).

2.3 M2-SCREAM Chemical Reanalysis

In addition to the L3 MLS products derived directly from MLS "Level 2" (L2, along orbit tracks) data and MERRA-2 meteorological information, we show some results for assimilated N_2O and H_2O from the recently available MERRA-2 Stratospheric Composition Reanalysis of Aura Microwave Limb Sounder (M2-SCREAM, Global Modeling and Assimilation Office (GMAO), 2022), which is described in detail by Wargan et al. (2022, submitted to ESSD). This reanalysis assimilates version 4.2 MLS L2 H_2O, N_2O, HCl, HNO_3, and ozone profiles (Livesey et al., 2018) using a constituent data assimilation system endowed with a full stratospheric chemistry module and driven by assimilated meteorological fields from MERRA-2. An earlier version of this assimilated product was used in a study of the 2019 Antarctic ozone hole (Wargan et al., 2020). As shown by Wargan et al. (2022), the assimilated species are in excellent agreement with MLS observations and realistically capture the spatial and temporal variability of these species. One advantage of the assimilated fields is that they provide synoptic high-resolution (same as that of MERRA-2 noted above) 3D gridded fields that are primarily controlled by the MLS observations.

2.4 Analysis Methods & Tools

In addition to the MLS L3 products, and a similar product giving vortex averages of ACE-FTS data produced on the fly using the MERRA-2 derived meteorological products described in Section 2.1 above, we calculate several quantities that are relevant to assessing transport characteristics. Horizontal potential vorticity (PV) gradients and effective diffusivity (K_{eff}, Nakamura, 1996) on isentropic surfaces derived from MERRA-2 provide indicators of mixing and transport barriers (e.g., Allen & Nakamura, 2003; Manney, Harwood, et al., 2009; Gille et al., 2014; Abalos et al., 2016; Manney & Lawrence, 2016). Diabatic heating rates from MERRA-2 and ensembles of thousands of trajectories provide information on diabatic descent, similar to that shown by Manney, Lawrence, Santee, Read, et al. (2015). The trajectories are calculated as in Lawrence et al. (2015) using MERRA-2 winds and diabatic heating rates as the inputs.

The primary results presented here are time series of anomalies from the 2005–2020 climatology of the trace gases. MLS version 4 H_2O and N_2O showed an instrument-related drift over the mission that has been ameliorated in v5 for H_2O, but only partially corrected for N_2O (Livesey et al., 2021); MLS time series have therefore been detrended by removing a linear fit over the mission to the L3 data for each day of year (for consistency, we detrend all species). For clarity, we focus in on 2010/2011 through 2019/2020 in the figures. 2010/2011 and 2015/2016 are of particular interest to compare with 2019/2020 because of the exceptionally strong and cold polar vortices in those years. For different reasons, 2012/2013 and 2013/2014 also provide valuable comparisons with 2018/2019 and 2019/2020. As discussed further below, this range of years covers those with the largest anomalies in the long-lived trace gas records we study herein.

"Level 3" products based on MLS data (described above in sections 2.2 and 2.3), that is, gridded products derived from the measurements along the orbit tracks, are critical to transport studies such as those herein. Both the MLS L3 products that provide a vortex-centered view (that is, vortex averages and equivalent latitude time series) and the high-resolution synoptic fields from the M2-SCREAM assimilated fields are invaluable in obtaining a view of transport that is continuous and well-resolved in space and time.

3 Overview of Fall/Winter/Spring Transport

Vortex averages of long-lived tracers throughout the stratosphere give a broad overview of transport within the vortex. Figure 1 shows cross-sections of v5 MLS H_2O, N_2O, and CO for 2010–2020. MLS vortex-averaged N_2O in 2019/2020 shows strong low anomalies in early winter between about 500 K and 700 K, which appear to progress downwards from the time of vortex formation through about mid-February, extending down to near 400 K by that time (note that 400 K is typically near or just below the lowest level at which the v5 N_2O data are considered scientifically useful). After that time, low anomalies persist and strengthen below about 550 K, and strengthen again at higher levels, up to about 700 K, in late February.

The evolution of vortex-averaged MLS H_2O shows nearly a mirror image of that in N_2O, with high instead of low anomalies. The high H_2O anomalies, however, never extend as low as 400 K and show an abrupt shift to near-zero or slightly low anomalies at the beginning of February around 450–500 K. This is consistent with the results of Manney et al. (2020), who showed that temperatures were below the ice polar stratospheric cloud threshold during this period and H_2O values abruptly decreased in the coldest portion of the vortex.

In 2010/2011, the previous Arctic winter with the strongest and most persistent stratospheric polar vortex, the anomalies in N_2O and H_2O are not obviously similar to those in 2019/2020, with slight high N_2O anomalies below about 700 K in early winter 2010/2011 (accompanying H_2O anomalies are near-zero), and descending low (high) anomalies in N_2O (H_2O) in the middle stratosphere beginning in January 2011. Note that, in 2018/2019, a major sudden stratospheric warming (SSW) occurred in early January (e.g., Butler et al., 2020), resulting in very high (low) N_2O (H_2O) anomalies in spring 2019; a similar event and pattern of anomalies occurred in the 2012/2013 winter (Manney, Lawrence, Santee, Livesey, et al., 2015). We will return to this point below.

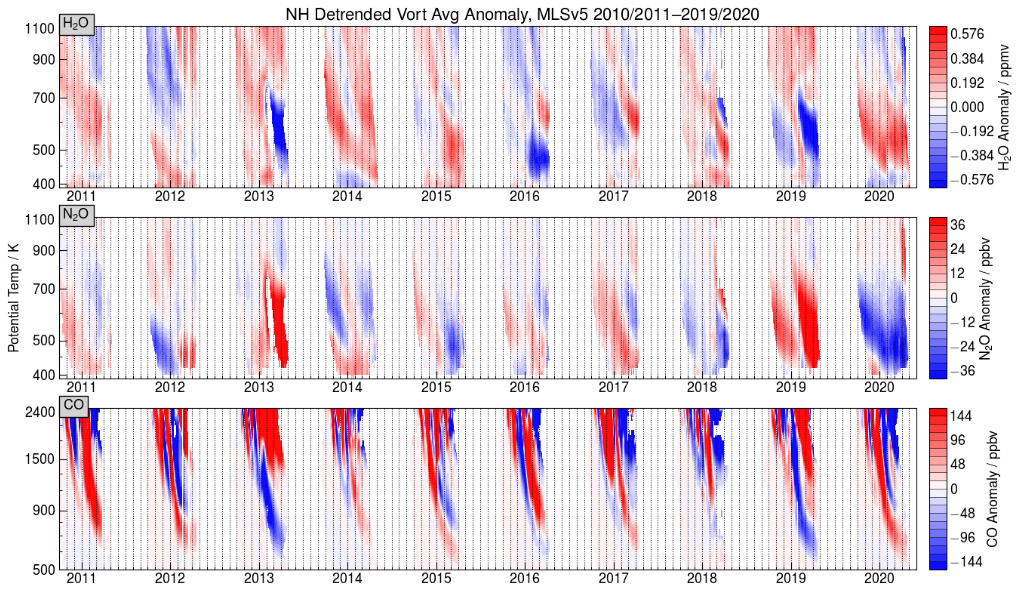

Figure 1. Time series of detrended anomalies from the 2005–2020 climatology of vortex-averaged MLS v5 H_2O, N_2O, and CO, shown for the 2010/2011 through 2019/2020 winters.

MLS vortex-averaged CO is shown over a vertical range from the lower stratosphere to the lower mesosphere (Figure 1). The largest signal in CO is from descent from the mesospheric vortex into the stratospheric vortex, which begins in fall (e.g., Manney, Harwood, et al., 2009; Manney, Lawrence, Santee, Read, et al., 2015; Lee et al., 2009; McDonald & Smith, 2013; Harvey et al., 2018). Large interannual and intraseasonal variability in this descent results from stratospheric and mesospheric polar vortex variations, and these differences (especially in vortex position and temporal evolution), coupled with near-zero CO abundances outside the vortex, lead to anomalies that can alternate rapidly from very high to very low. However, the envelope of anomalies that extend below the middle stratosphere provides a good indication of interannual variations in the overall winter-long descent from the mesosphere. 2019/2020 is remarkable in this respect, showing descent of high CO to the lowest altitudes seen in the Aura MLS record. A similar pattern of anomalies was seen in 2010/2011, although the envelope is not fully defined in that year because of the MLS data gap from late March to mid-April; nevertheless, at the time of the onset of that gap, high CO anomalies already extended to lower levels in 2020 than in 2011. High CO anomalies extending to similarly low altitudes (but of smaller magnitude) were also seen in 2014/2015, a winter characterized by a prolonged period with anomalously strong descent within an unusually strong (but not cold) vortex (Manney, Lawrence, Santee, Read, et al., 2015). The early January SSWs in 2013 and 2019 resulted in the opposite extremes, with low anomalies in overall winter descent of CO (and subsequent lower mesosphere/upper stratosphere high anomalies as descent from the mesosphere intensifies during reformation of the upper stratospheric vortex, as described for 2013 and earlier events by, e.g., Manney, Schwartz, et al., 2009; Manney, Lawrence, Santee, Read, et al., 2015; Harvey et al., 2018). ¿

We confirm and augment the vortex-averaged results from MLS using ACE-FTS data. As discussed by Manney et al. (2007) and Santee et al. (2008), "vortex averages" from ACE-FTS are typically not representative of the entire vortex (particularly when is it more circular and pole-centered as it was in 2019/2020), since the occultations (sunrise or sunset) are made at one latitude each day. Figure 2 shows a representative example at one level comparing MLS and ACE-FTS vortex averages of the species discussed herein, along with time series of the number of ACE-FTS measurements obtained within the vortex each day, and the average sPV (scaled PV, e.g., Dunker-

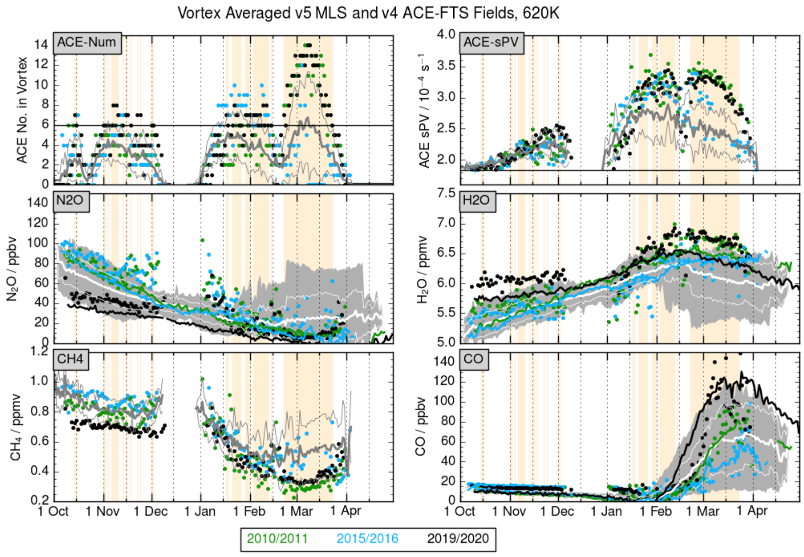

Figure 2. Time series at 620 K showing the number and sPV values of ACE-FTS measurements within the vortex, along with MLS v5 and ACE-FTS v4 N_2O, H_2O, CH_4 (ACE-FTS only), and CO, for the 2004/2005 through 2019/2020 Arctic winters. 2010/2011, 2015/2016, and 2019/2020 are highlighted in green, cyan, and black, respectively, and are omitted from the ranges and means over the other years. Light tan shading shows date ranges in 2019–2020 with six or more ACE-FTS measurements within the vortex. Grey shaded regions on the panels with MLS data show the MLS range; on ACE-FTS-only panels, thick grey lines show the mean over the years that are not highlighted and thin grey lines indicate the range of values over the those years. (Note that MLS values here are not detrended, so they may show apparent inconsistencies with the detrended anomalies.) The horizontal line on the upper left denotes six measurements inside the vortex; the horizontal line on the upper right demarks the sPV value used for the vortex edge.

ton & Delisi, 1986; Manney et al., 1994) values of those measurements. The latter quantity provides a measure of how far inside the vortex the measurements are. Because the ACE-FTS orbit repeats nearly the same sampling each year, the overall patterns are similar most of the time but do vary depending on the vortex size, shape, and position (the average over the mission is shown in panels that do not also show MLS data). In 2019/2020, the only extended periods of more than a few days with more than six measurements per day within the vortex are during early November, late January to late February, and mid-February to late March. During those periods, the MLS and ACE-FTS trace gas measurements generally show consistent time evolution for the species shown.

Cross-sections of vortex-averaged ACE-FTS N_2O and H_2O (Fig. 3) generally show behavior that is consistent with that seen in MLS. These fields come closest to representing the same conditions as those from MLS in the periods shown above when there are most ACE-FTS measurements inside the vortex and those measurements are situated toward the interior of the vortex and away from its edge. With this caveat in mind, the ACE-FTS H_2O and N_2O vortex averages show good agreement with those from MLS from the lower through the middle stratosphere. Above about 800 K, ACE-FTS shows high H_2O anomalies in 2019/2020 at times / heights where MLS shows (typically weak) negative anomalies; similar features with low anomalies in MLS fields but high ones in ACE-FTS fields are seen in several previous seasons (e.g., for the years shown here, in 2014/2015, 2016/2017, and 2017/2018), especially in spring. Examination of levels above those shown here indicates that the difference between MLS and ACE-FTS H_2O in 2019/2020 extends from about 800 K through 1200 K. It is likely that this is primarily related to the inter-

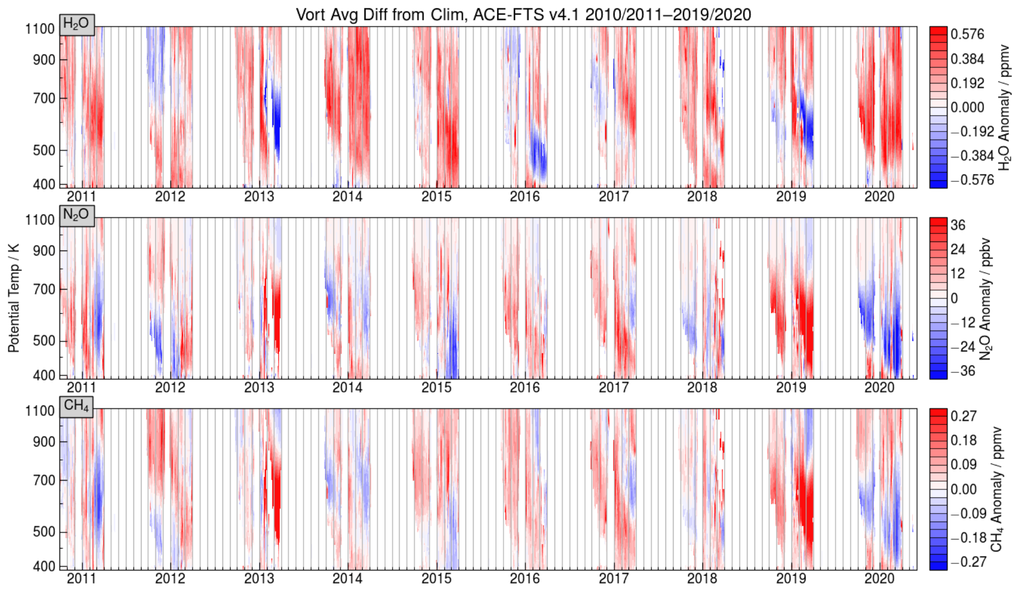

Figure 3. Time series of anomalies from the 2005–2020 climatology of vortex-averaged ACE-FTS v4.1 H_2O, N_2O, and CH_4, shown for the 2010/2011 through 2019/2020 winters.

play between instrumental sampling patterns and vortex variations (arising from minor warmings or earlier onset of disturbances leading to its final breakup in the upper stratosphere) that change the relationship between the MLS and ACE data coverage. Vortex-averaged CO from MLS and ACE-FTS agree well during periods when ACE-FTS has relatively good vortex sampling (see Fig. 2 and discussion above), consistent with good agreement in cross-sections of vortex-averaged CO anomalies from the two instruments (not shown). Because N_2O and CH_4 are both long-lived tracers with tropospheric sources, their vertical and horizontal gradients are in the same direction; thus the very similar patterns in ACE-FTS CH_4 anomalies confirm the patterns seen in N_2O from both instruments and add further weight to the supposition that these anomalies arise from unusual transport within the vortex.

To provide a more complete view of the transport anomalies associated with the 2019/2020 Arctic vortex in a hemispheric context, Figs. 4 through 7 show detrended MLS anomalies from climatology as a function of equivalent latitude (the latitude that would enclose the same area between it and the pole as a given PV contour, Butchart & Remsberg, 1986) and time at several levels. To relate the observed patterns to mixing and transport barriers, we also show anomalies in K_{eff} and in horizontal sPV gradients calculated from MERRA-2.

At 500 K (Fig. 4), 2019/2020 shows the largest negative anomalies in K_{eff} and positive anomalies in sPV gradients in the years of the Aura mission, with these anomalies becoming apparent as soon as the vortex forms, around late November at this level. 2010/2011 shows similar anomalies, but they are weaker and not consistently negative (positive) for K_{eff} (sPV gradients) before mid-January. In 2013/2014, another winter with a relatively robust vortex throughout the season, a pattern of anomalies similar to that in 2019/2020 is evident until an earlier vortex breakup. The opposite extreme is seen in the 2012/2013 and 2018/2019 winters, both of which show large-magnitude weak vortex anomalies (high K_{eff}, low sPV gradients) after SSWs followed by brief periods of inverse anomalies in spring when the vortices partially reform.

Consistent with the exceptional vortex confinement, H_2O and N_2O anomalies in 2019/2020 at 500 K (Fig. 4) are high and low, respectively, throughout the period when the vortex exists, with the strongest anomalies in spring (when the vortex has already broken up or is breaking up in most

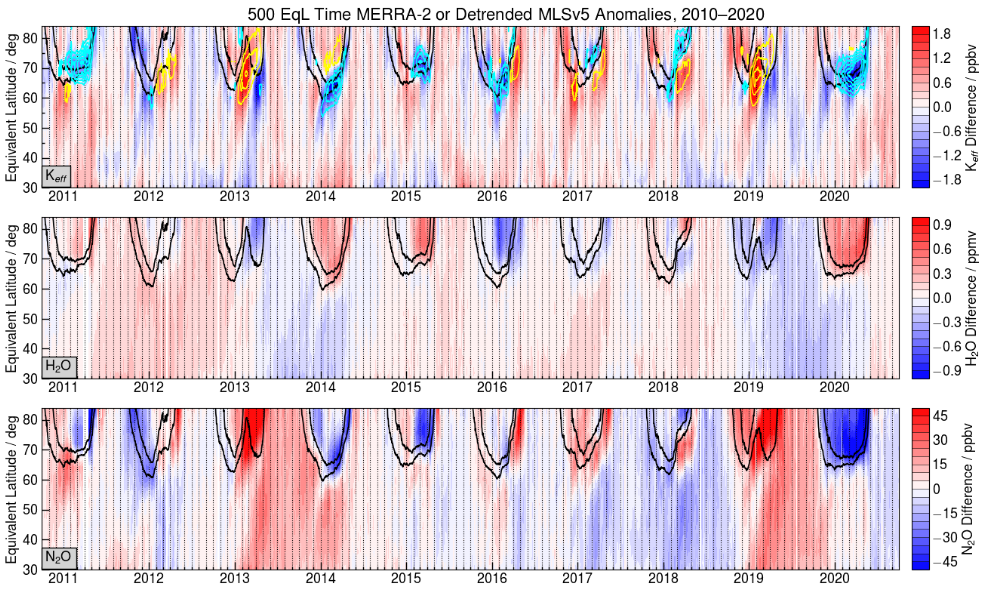

Figure 4. Time series at 500 K (about 20–21 km) of anomalies from the 2005–2020 climatology of MERRA-2 effective diffusivity (K_{eff}) and detrended MLS v5 H_2O and N_2O, shown for the 2010/2011 through 2019/2020 winters. Black overlays are scaled PV (sPV) contours of 1.4 and 1.8 $\times 10^{-4}$ s^{-1}, demarking the vortex edge region. Cyan (yellow) overlays on the K_{eff} anomaly plots are positive (negative) anomalies from climatology of horizontal sPV gradient with respect to equivalent latitude.

previous years). Similar (though weaker) spring anomalies are seen in 2011, but they followed weak anomalies of the opposite in early winter, consistent with the later onset of anomalous vortex strength in that winter than in 2019/2020. The hemispheric patterns of N_2O in early 2013 through spring 2014 are remarkably similar to those in early 2019 through spring 2020, with pervasive high N_2O anomalies throughout the hemisphere starting in January 2013 and 2019 and persisting outside the vortex through the early months of 2014 and 2020; anomalies of opposite sign are also seen in H_2O, though the anomalies are both weaker and arise slightly later in 2013 than in 2019. Though the 2013/2014 vortex was not as strong or long-lived as that in 2019/2020, it also was characterized by high (low) H_2O (N_2O) anomalies through most of the winter. This pattern could arise either from exclusion of low (high) H_2O (N_2O) values from the vortex as it formed or from descent of anomalous values from above (resulting from either stronger descent or more extreme values at higher levels). Together with the anomalies in mixing and transport barriers, the patterns of transport in the entire extratropical Northern Hemisphere at this level from early 2013 through spring 2014 are remarkably similar to those from early 2019 through spring 2020. (Several other January SSWs occurred in the Aura timeframe in addition to those in 2013 and 2019, but none of the others showed patterns similar to these in relation to the following winters, nor pervasive hemispheric anomalies persisting from one winter to the next.)

A similar overall picture is seen in 2019/2020 at 620 K (Fig. 5), with a corresponding pattern of anomalies in K_{eff} and sPV gradients. However, at this level pervasive low anomalies in N_2O and (weaker) high anomalies in H_2O appear in spring 2019 and persist through that summer and into fall throughout the Northern Hemisphere extra-tropics. Conversely, patterns in spring through fall 2013 at this level shows high N_2O anomalies similar to those at 500 K and weak H_2O anomalies that shift from negative to positive depending on the time. Thus at 620 K, fall 2019 is unique in that the vortex develops in an environment with existing N_2O and H_2O anomalies

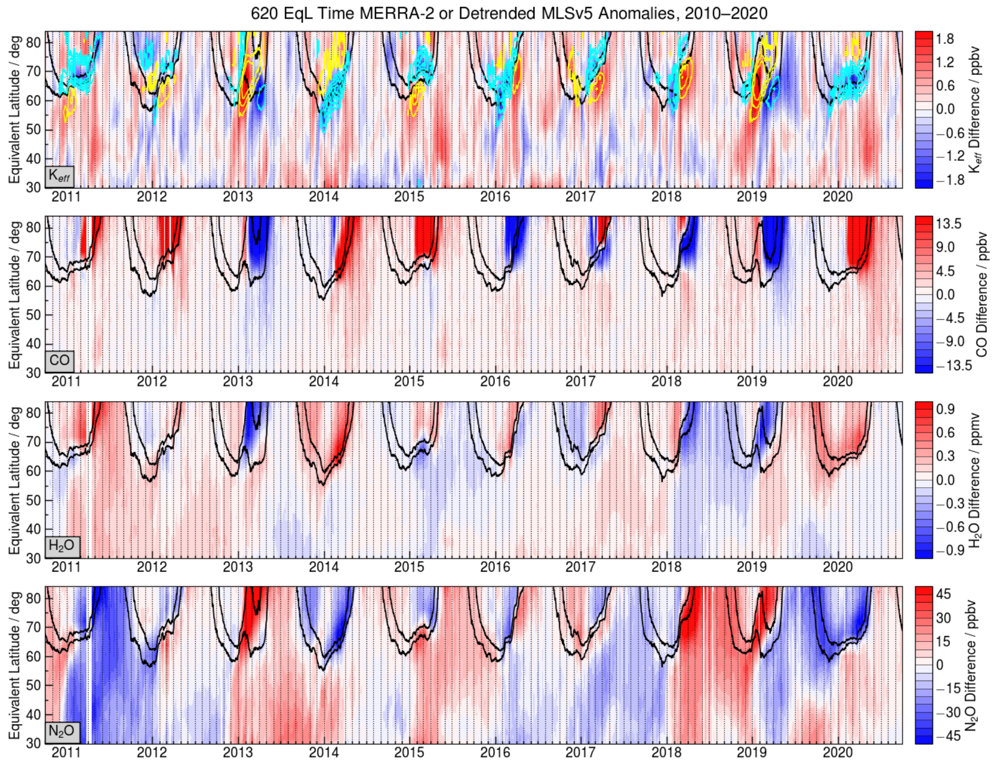

Figure 5. As in Fig. 4, but at 620 K (about 24–25 km) and also showing MLS v5 CO anomalies.

of the same sign as those that would be expected to develop via descent within an exceptionally strong (and hence less permeable) vortex.

Figure 5 also shows CO anomalies. Consistent with the particularly long-lived vortices, strong high CO anomalies are seen in the springs of 2011, 2014, and (the strongest) 2020. Similar high anomalies are seen in 2012 and 2015; though the vortices in those winters were not overall as continuously robust or long-lived as in the years mentioned above, they did have relatively late breakups at this level. Thus in all of the years with high CO anomalies, descent within the confined vortex persisted longer, allowing larger abundances to reach lower altitudes. These anomalies are associated with high anomalies that spread through the hemisphere as the vortex breaks up in spring. The opposite extreme is seen in spring 2013 and 2019, with low CO anomalies in the vortex because the signature of confined descent was interrupted by SSWs and consequent dispersal of low anomalies as the vortex breaks up. The timing of onset of the high CO anomalies varies among the years shown here, but is earliest in 2015 and 2020, implying either larger mid-winter through spring descent rates (as was the case in 2015, Manney, Lawrence, Santee, Read, et al., 2015) or descent of higher values.

The patterns of long-lived trace gas anomalies evolve gradually with increasing height. Moving up to 700 K (Fig. 6), the anomalies in 2018/2019 through 2019/2020 are similar to those at 620 K. At this level (unlike at 620 K), 2012/2013 through 2013/2014 show patterns of both H_2O and N_2O anomalies that parallel those in 2018/2019 through 2019/2020: high (low) anomalies in H_2O (N_2O) appear from the subtropics through midlatitudes (below 60°N equivalent latitude) shortly after the SSWs (and accompanying anomalies of the opposite sign). These anomalies progress to fill middle to polar latitudes (near 40°N equivalent latitude to the pole) in spring and persist through summer and the following fall. While there were generally high (low) H_2O (N_2O) anomalies in the vortex throughout its existence in both 2013/2014 and 2019/2020, they were much weaker

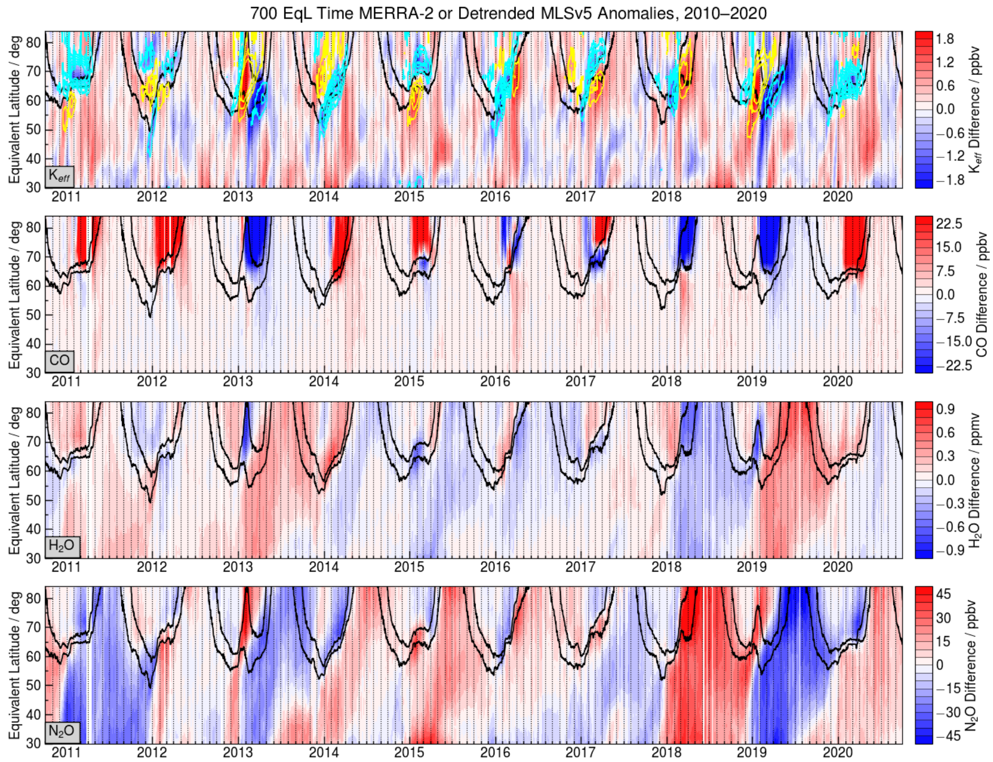

Figure 6. As in Fig. 5, but at 700 K (about 27–28 km).

than at lower levels and showed brief periods of near-zero or oppositely signed anomalies. Similar patterns in H_2O and N_2O are seen at higher levels through about 1000 K. The patterns of CO anomalies are similar to those already discussed at 620 K (except in 2015 when they were less persistent at this level), with the strongest anomalies again seen in 2020; these patterns of CO anomalies are also similar at higher altitudes.

Figure 7 shows a view of the upper stratosphere (N_2O is not shown at this level because most values are low enough that they are near / less than the precision of the MLS measurements even in these daily averages). At this level, 2019/2020 does not stand out as having a unique pattern of anomalies. As seen in the sPV contours and gradients and in K_{eff}, most winters show both strong and weak vortex anomalies at different times throughout the season. The timing of the vortex breakup in spring (as indicated by the overlaid sPV contours) is not unusual in either 2011 or 2020 at this level. As seen in the K_{eff} anomalies, both 2010/2011 and 2019/2020 are among the years with minor SSWs in January or February with effects that were confined to / above the upper stratosphere. Upper stratospheric and mesospheric disturbances in late January to February 2020 are discussed by Ma et al. (2022) and Lukianova et al. (2021); while similar disturbances often precede major SSWs, both studies discussed conditions surrounding these events that facilitated the persistence of the exceptionally strong vortex at lower altitude, in the middle and lower stratosphere. Consistent with the unremarkable vortex evolution at this altitude, the behavior of MLS CO and H_2O was not particularly unusual 2019/2020. That 2019/2020 does not stand out at this level indicates that the uniquely strong trace gas anomalies in the middle and lower stratosphere in that year do not result directly from descent of upper-stratospheric or mesospheric anomalies.

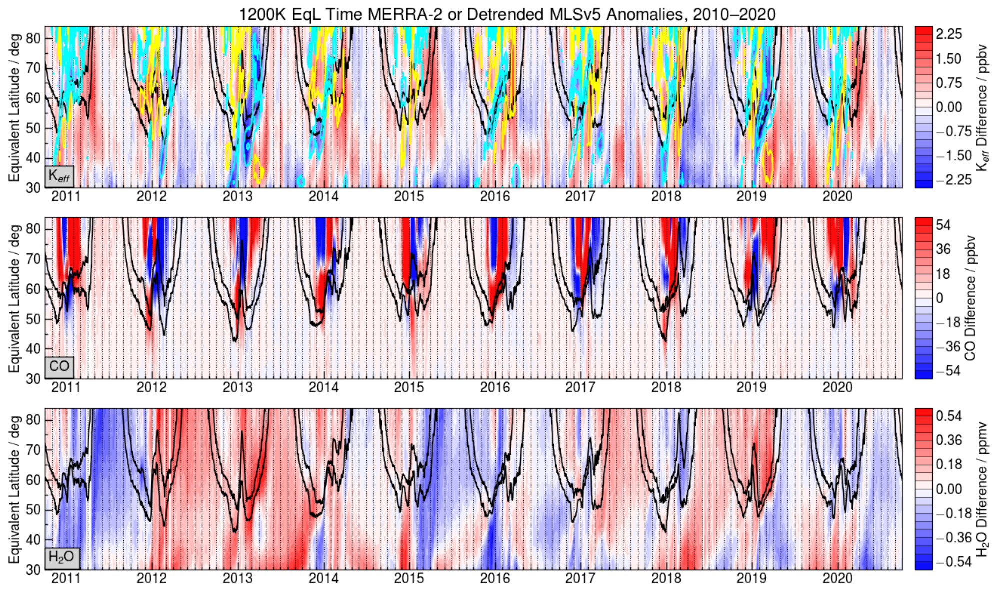

Figure 7. As in Fig. 5, but at 1200 K (about 38–40 km) and showing only MLS v5 CO and H_2O. sPV gradient contour interval is twice that at the lower levels.

4 Discussion

4.1 Vortex Development and Confined Transport in Fall through Midwinter

The patterns of unusually low N_2O and high H_2O in the middle and lower stratospheric vortex in fall through midwinter appear to be consistent with either anomalies in descent within the vortex (either via more diabatic descent or descent of air already lower (higher) in N_2O (H_2O)) or with less mixing than is typical of extra-vortex air into the vortex.

An overview of diabatic descent anomalies is given in Fig. 8, which shows differences from climatology in descent rate (total diabatic heating; negative values indicate diabatic descent) from MERRA-2 in recent winters. The anomalies in descent rates in fall to early winter (through middle to late December) are typically small and do not stand out as unusual in 2019/2020 or in 2010/2011 (for instance, compare the rates in those years with the consistently stronger descent in fall 2011 and consistently weaker descent in fall 2016). In both the 2010/2011 and 2019/2020 fall / early winter periods, anomalies vary from weakly negative to weakly positive from week to week. A similar pattern was seen in the 2015/2016 middle and lower stratosphere until late February, when the behavior of the until-then record-cold vortex began to diverge from that in the years that remained cold much later into spring. Starting in February in both 2010/2011 and 2019/2020, anomalously strong descent is seen in the middle to upper stratosphere (above about 700 K). There was a brief increase in anomalous descent (larger negative values) in 2019/2020 concurrent with the early February 2020 minor SSW that affected the upper stratosphere and mesosphere. This overview of diabatic heating/cooling averaged within the vortex does not support significant anomalies in descent rates in fall through midwinter in 2019/2020. This is consistent with the evidence shown above that the trace gas anomalies are largely confined to the middle and lower stratosphere and do not arise primarily from anomalous descent.

Because the vortex-averaged gridded descent rate values shown above do not necessarily represent the rates experienced by individual air parcels as they move around within, or in some cases (particularly in fall) are entrained into, the vortex, we also examine the history of air parcels within the vortex on several days for 2019/2020 compared with previous winters during the Aura

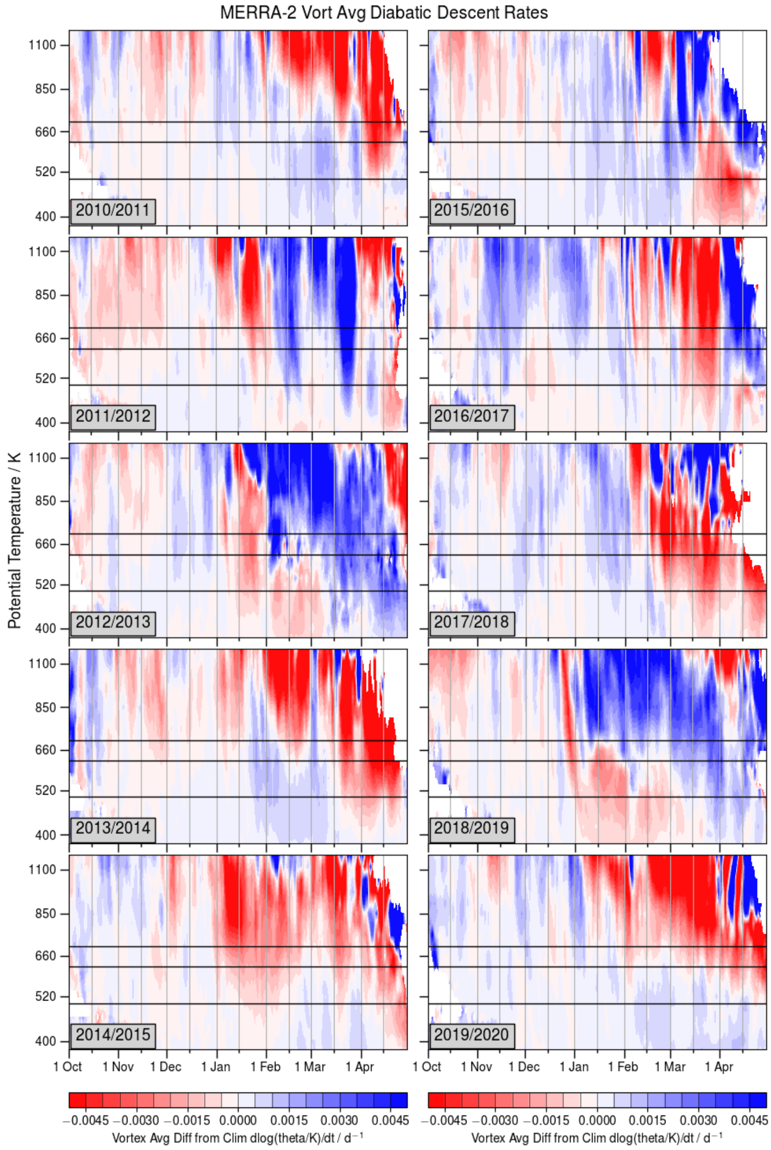

Figure 8. Cross-sections of anomalies from the 2005–2020 climatology of vortex-averaged diabatic heating/cooling rates from MERRA-2 for October through April in 2010/2011 through 2019/2020. Rates are expressed as dln(θ)/dt. Overlaid lines mark 500, 620, and 700 K. Note that the color scale has been inverted (negative values are reds) to emphasize anomalies indicating unusually strong descent.

mission; Fig. 9 shows representative examples. Neither lower nor middle stratospheric descent in early winter (through December) shows strong interannual variability, nor do any of the four cold winters highlighted show consistently atypical behavior. Interannual variability is much larger throughout the midwinter to spring period, but, again, 2019/2020 does not stand out as showing particularly anomalous descent. Parcels inside the vortex at 800 K at the end of January 2020 had, indeed, experienced unusually strong descent in early through mid-November 2019, but, since H_2O anomalies at higher levels (e.g., see Fig. 7) were slightly low prior to and during vortex development in 2019, the atypical early-winter descent could not explain the high H_2O anomalies within the vortex at lower levels. (In addition, even stronger descent was experienced at that time by parcels at 800 K at the end of January 2011, when there was no such signature of anomalous descent.) These more quantitative results are consistent with Figs. 1 and 3 in that anomalous values of the vortex-averaged trace gases were apparent as soon as the vortex formed and appeared to descend at a fairly typical rate. The descent rates shown here also appear to be consistent with calculations of vortex-averaged descent from MLS N_2O done by Manney et al. (2020), which did not show obvious anomalies in 2020.

Regarding the possible role of mixing, the K_{eff} panels in Figs. 4 through 6 (and up through about 1000 K, not shown) do show negative anomalies (and positive sPV gradient anomalies) indicating reduced mixing starting in November, while the vortex is still developing / strengthening. These anomalies are, however, relatively small until the end of 2019. Thus, although less mixing into the vortex might have contributed to the early-winter anomalies, the most likely origin for them appears to be the entrainment into the vortex above about 650 K of already anomalous H_2O and above about 600 K of already anomalous N_2O abundances, followed by descent (at a relatively typical rate) of those anomalies to lower levels.

Figure 6 shows clearly that the high (low) H_2O (N_2O) anomalies that were entrained into the vortex in fall 2019 (and also in fall 2013) arose during the winter to spring of those years following a brief period of anomalies of the opposite sign immediately after early-January major SSWs. The low (high) H_2O (N_2O) anomalies immediately following the SSWs are consistent with enhanced mixing of extra-vortex air into high latitudes as the vortex weakens or breaks down and are also seen following other strong SSWs in the Aura record (e.g., the later January 2006 and 2009 SSWs (not shown), Manney, Harwood, et al., 2009; Manney, Schwartz, et al., 2009). The subsequent rapid onset of high (low) H_2O (N_2O) anomalies, beginning concurrently with the SSWs at low equivalent latitudes and spreading through the Northern Hemisphere by April (when the vortex disappears), is seen in the Aura record only in 2013 and 2019. While investigation of the causes of these unusual spring-through-fall trace gas anomalies is beyond the scope of this paper, ongoing studies suggest a relationship with Quasi-biennial oscillation (QBO) phase. These two years show westerly shear in QBO winds near 600–700 K during the Northern Hemisphere fall and early winter, in contrast to other years in the record, in which the shear is easterly or close to neutral. This westerly shear (along with vortex disruption by early SSWs) may be responsible for the high (low) H_2O (N_2O) anomalies that propagate from the tropics poleward, consistent with known QBO tracer transport effects (e.g., Baldwin et al., 2001).

4.2 Vortex Persistence and Breakup in Spring

In contrast to the evolution of long-lived trace gas anomalies in fall and early winter, their persistence and progression from mid-February through the vortex breakup in spring is best explained by the unprecedented strength of the vortex in 2020 and consequent inhibition of mixing between vortex and extravortex air. As can be seen in the overlaid sPV contours in Figs. 4 through 6, the vortex persisted through April in the middle stratosphere and into May in the lower stratosphere. Figure 10 shows maps of N_2O and H_2O from the M2-SCREAM chemical reanalysis during the period leading up to the vortex breakup in 2019/2020 at one level in the middle stratosphere (700 K) and one level in the lower stratosphere (520 K), providing a high-resolution view of the breakup and the fate of the vortex remnants in fields with information content based primarily on MLS data.

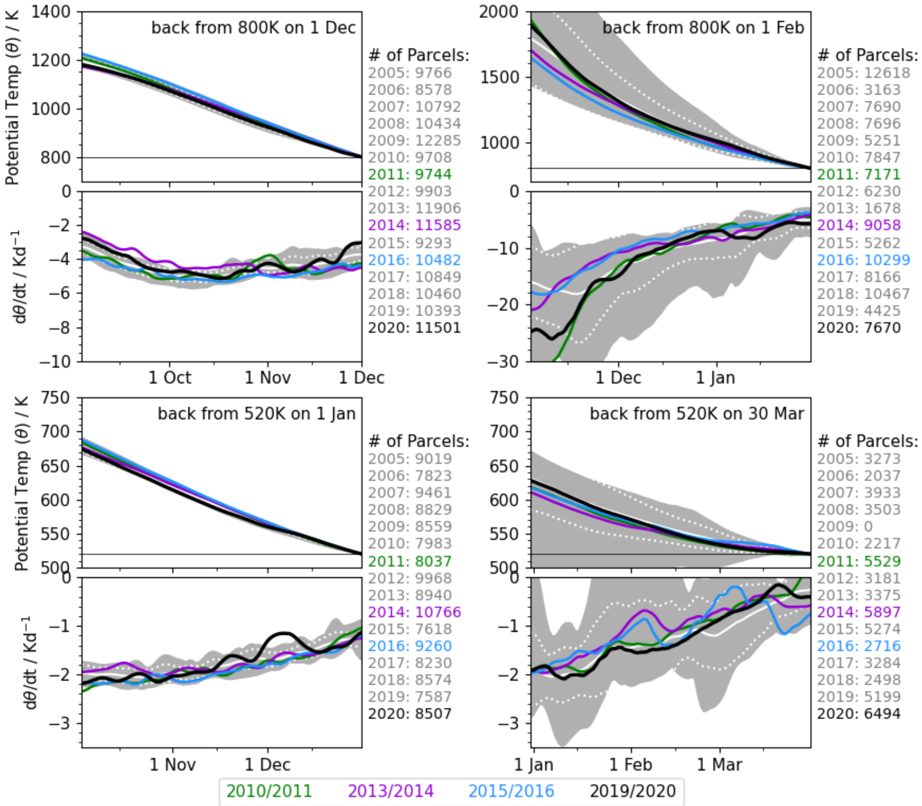

Figure 9. Descent over the preceding 90 days to 800 K (top pairs of panels) and 520 K (bottom pairs of panels) on the final day, from 1 December (left) and 1 February (right) for 800 K and from 1 January (left) and 30 March (right) for 520 K, from back-trajectory calculations initialized on a dense equal-area grid throughout the vortex (see text, Section 2). Grey shading shows the range for 2004/2005 through 2018/2019, excluding the years that are highlighted (2010/2011, 2013/2014, 2015/2016, and 2019/2020); white solid line shows the mean and white dashed lines the one standard deviation range. Top panel in each pair shows the overall descent; bottom panel shows the descent rate (dθ/dt) calculated from that. The number of parcels inside the vortex on the initialization (latest) date in each year is shown to the right of each set of panels; since the initialization grid is equal-area, this value indicates the relative size of the vortex on the initialization day.

A vortex-split event occurred in the middle and lower stratosphere around 22 April 2020 (the second day shown here), in the period leading to the vortex breakup. In their analysis of this event, Curbelo et al. (2021) focused on transport within the vortex at a level near that shown for the lower stratosphere here, identifying transfer of air from well inside the main (larger) vortex to the offspring vortex. Though they did not describe transport into or out of the vortex, their results are consistent with what we see here; that is, into late April in the middle stratosphere and about mid-May in the lower stratosphere, the air within the vortex is extremely well-confined, with very little evidence of dispersal from the vortex. In the middle stratosphere, filaments are being drawn off the vortex by mid-April (14 April is shown here) but, except for these narrow filaments, the gradients across the edge of the vortex or its main remnant remain very strong through early May, and a vortex remnant of substantial size persists through about 8 May 2020 at 700 K. In the lower stratosphere, the vortex (or sizeable remnants thereof) remains well-defined and continues to have exceptionally strong trace gas gradients across its edge through mid-May (e.g., 16 May shown here); by 8 May there are suggestions of a small amount of mixing of lower (higher) N_2O (H_2O) air out of the vortex associated with some filamentation, but only a small amount of material is likely carried by these streamers. The surviving (larger) vortex after the 22 April split moves over Siberia and Asia. Curbelo et al. (2021) show that the lowest ozone mixing ratios remain in that main vortex during the split; the position of the vortex, and after the split the position of this larger remnant, is consistent with the substantial low anomalies in column O_3 (and accompanying high anomalies in surface ultraviolet radiation) seen in that region in May 2020 monthly means (Bernhard et al., 2020).

4.3 Related Upper Troposphere / Lower Stratosphere Composition Anomalies

Anomalies in the stratospheric polar vortex (both SSWs and strong vortex states, though the former have been far more studied) have been shown to be linked to circulation anomalies extending down to the surface (Kidston et al., 2015; Domeisen & Butler, 2020, and references therein). Stratospheric polar vortex composition variability can also strongly influence extratropical stratosphere/troposphere exchange (STE); for example, Albers et al. (2018) showed that ozone concentrations in the lower stratospheric reservoir in spring are a critical factor controlling the amount of ozone transport into the troposphere through the following summer. We thus briefly examine how ozone anomalies associated with the exceptional strength of the Arctic stratospheric vortex in 2019/2020 may be reflected in UTLS fields.

Figure 11 shows equivalent latitude time series of O_3 at three levels in the UTLS. At 370 K, the tropopause crosses isentropic surface just north of 30°N, so the extratropics are in the lowermost stratosphere. Strong low anomalies in O_3 are seen in winter/spring 2016 and 2020; the somewhat weaker low anomalies in spring 2011 are consistent with the ozone loss peaking at and extending to lower altitudes in 2020 than in 2011, and suggests that chemical loss extends down to this level in 2020. Indeed, (Wohltmann et al., 2020, 2021) showed evidence that chemical loss in 2020 extended down to at least 370 K, below which their calculations were not robust, and Manney et al. (2020) showed chemical ozone loss in 2020, but not that in 2011, extending below 400 K. Fig. 8 shows small but persistent low anomalies in descent at and below 400 K in February through April 2020, and similar anomalies in February through March 2011, and February through mid-March in 2016 and 2014. This suggests that weaker than usual descent contributes to the lower 370 K ozone in addition to descent of lower ozone abundances and some in situ chemical loss. In 2011 and 2020 the low ozone anomalies persisted into summer, indicating very low ozone in the lowermost stratospheric reservoir.

At 330 K and 340 K (Fig. 11), strongest low ozone anomalies are seen in late 2019/2020 and persist into spring after the overlying stratospheric vortex has broken up. The extension of these anomalies across the tropopause suggests an impact on extratropical STE. High anomalies in 2013 and 2019, and at higher equivalent latitudes or for shorter periods in 2015 and 2018, are consistent with the higher ozone values in the overlying stratosphere resulting from a variety of SSWs (e.g., Manney, Lawrence, Santee, Livesey, et al., 2015; Manney, Lawrence, Santee, Read, et al., 2015; Butler et al., 2020). They also appear (except in 2015) to be accompanied by

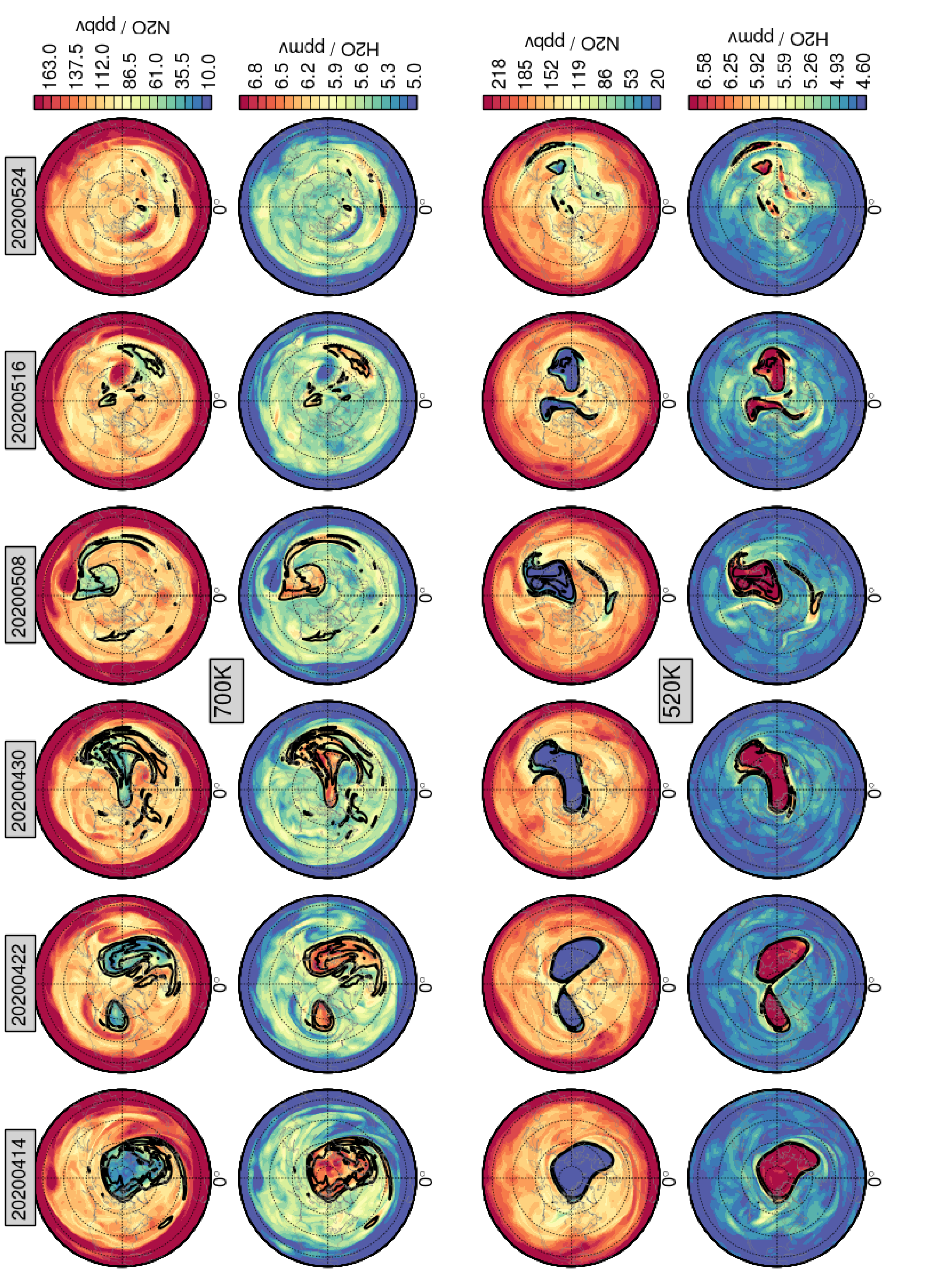

Figure 10. Maps of N_2O and H_2O in the middle (top rows, 700 K) and lower (bottom rows, 520 K) stratosphere from the M2-SCREAM reanalysis during the 2020 spring vortex breakup.

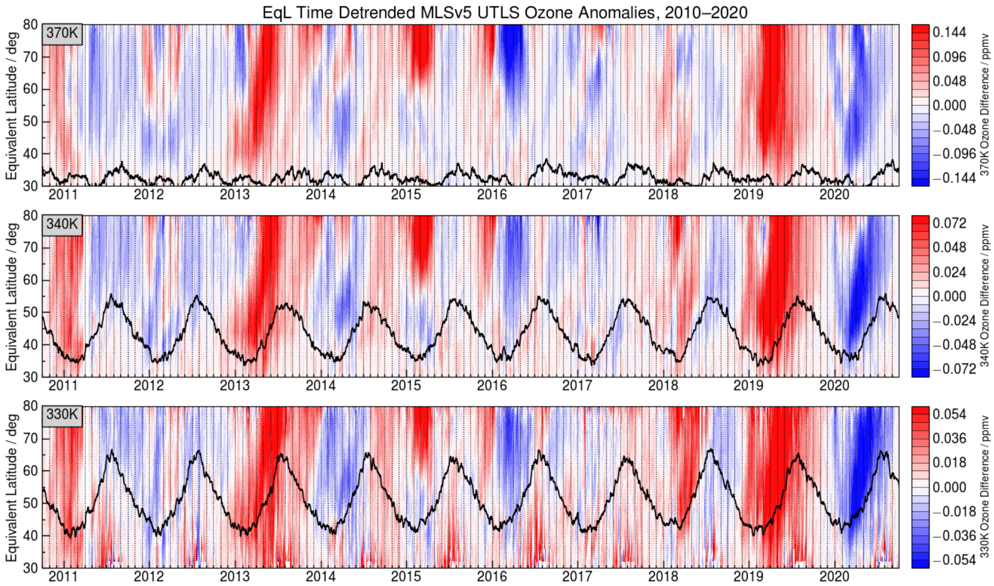

Figure 11. Equivalent latitude time series for 2010/2011–2019/2020 showing ozone at 370 K (top), 340 (center), and 330 K (these levels span approximately 10 to 15 km altitude). Black contour shows location of 4.5 PVU dynamical tropopause.

transport of anomalously high ozone into the troposphere, consistent with the findings of Albers et al. (2018). The origin of the high O_3 anomalies in early 2011 is unclear, as overlying stratospheric ozone was unusually low; further investigations beyond the scope of this paper will be required to understand this feature.

5 Summary and Conclusions

Aura MLS measurements, along with measurements from ACE-FTS and reanalyses, are used to give a comprehensive overview of anomalous transport in and around the exceptionally strong Arctic stratospheric polar vortex in the 2019/2020 fall, winter, and spring, in comparison with previous winters in the MLS and ACE-FTS records. Unique anomalies are seen, particularly in the lower and middle stratosphere, in the distributions of long-lived trace gases including N_2O, H_2O, CO, and (from ACE-FTS) CH_4 throughout the vortex season from before its development to after its breakup in spring. Our major findings include:

The Arctic stratospheric polar vortex in 2019/2020 was the strongest in the Aura record according to numerous metrics (see also Lawrence et al., 2020, for discussion of vortex strength in relation to longer-term records). We showed herein low anomalies in effective diffusivity throughout the vortex season, with the largest low anomalies on record from December or January (depending on the level) through the late vortex breakup in spring. These, coupled with the strongest potential vorticity gradients on record during the same period, indicate strongly inhibited mixing between vortex and extravortex air. This unprecedented vortex confinement extended from the lower (below 400 K) through the middle stratosphere (up to about 1000 K).

Record-low anomalies in N_2O and high anomalies in H_2O were seen throughout the season in the lower through middle stratosphere. Such anomalies could arise either from anomalous descent (which in turn could arise either from the rates or the abundances of trace gases being carried down or both) or from the inhibited mixing described above. In fall and early winter, the strongest low anomalies are found between about 550 K and 800 K and appear to progress downward with time through January 2020. Examination of descent during this period indicates that the proximate cause of the fall/winter anomalies and their subsequent descent was not anomalous descent rates but rather the descent of low (high) N_2O (H_2O) values that were entrained during vortex development from anomalies already pervading the northern extratropics through the preceding summer and into the fall. These preexisting anomalies appear to be associated with anomalous values that developed following the early January SSW in 2019, which may result from westerly shear associated with the QBO near 600–700 K at the beginning of those winters. Similar but weaker anomalies were seen following the SSW in early January 2013; they also persisted through that summer and the vortex development in fall 2013. Understanding the mechanisms responsible for such long-lasting anomalies that persist from spring through fall is a subject of ongoing research.

The anomalies in spring 2020 arise primarily from the record-breaking strength and persistence of the vortex, via the inhibition of mixing between vortex and extravortex air, and the longest persistence of that transport barrier on record in the Arctic in over 40 years (Lawrence et al., 2020). Anomalies resulting from the remarkably impermeable and long-lived Arctic vortex include not only the persistence of strong low (high) N_2O (H_2O) anomalies, but also high CO anomalies extending down to about 600 K arising from the extreme inhibition of mixing between vortex and extravortex air as CO descended from the mesosphere through the upper stratosphere. Examination of high-resolution maps of assimilated MLS N_2O and H_2O showed exceptionally effective confinement of trace gases within the middle (lower) stratospheric vortex through late April (mid-May) 2020. The main lower-stratospheric vortex remnant (containing the air most depleted in ozone Curbelo et al., 2021) lingered over Siberia and Asia through mid-May, consistent with the location of May column ozone anomalies.

Trace gas anomalies in the upper stratosphere, as well as many of those in the UTLS, were less remarkable and not obviously specifically related to the exceptionally strong polar vortex. Transport of O_3 and O_3 STE, however, were strongly affected by the record-low ozone in the reservoir in the lowermost stratosphere that may be transported into the troposphere.

The dramatic transport anomalies linked to the exceptionally strong and persistent 2019/2020 stratospheric polar vortex could only be diagnosed using a long record of daily global measurements of long-lived trace gases such as that from MLS. These long-lived trace gas measurements (augmented by sparser measurements from ACE-FTS), and reanalyses assimilating them, are invaluable tools for understanding the interannual variability of and changes in transport. Understanding of these transport effects is in turn critical to understanding chemical and radiative processes (e.g., ozone depletion and changes in trace gas distributions that have large radiative impacts), as well as to improving our ability to model these processes.

6 Open Research

The data used herein are publicly available as follows:

- MERRA-2: (Global Modeling and Assimilation Office (GMAO), 2015) `https://disc.sci.gsfc.nasa.gov/uui/datasets?keywords=%22MERRA-2%22`
- Aura MLS Level-2 and Level-3 data: (Lambert, Read, & Livesey, 2020; Lambert, Livesey, & Read, 2020; Lambert et al., 2021b, 2021a; Schwartz, Pumphrey, et al., 2020; Schwartz, Froidevaux, et al., 2020; Schwartz, Pumphrey, et al., 2021; Schwartz, Froidevaux, et al., 2021) `https://disc.gsfc.nasa.gov/datasets?page=1&keywords=AURA%20MLS`
- ACE-FTS v4.1 data: `http://www.ace.uwaterloo.ca` (registration required)
- ACE-FTS v4.1 error flags: `https://dataverse.scholarsportal.info/api/access/dataset/:persistentId/versions/:latest?persistentId=doi:10.5683/SP2/BC4ATC`
- MLS & ACE-FTS derived meteorological products: `https://mls.jpl.nasa.gov/eos-aura-mls/dmp` (registration required).

- M2-SCREAM: (Global Modeling and Assimilation Office (GMAO), 2022)
  (URL to be activated before 8 July)

Acknowledgments

Thanks to the MLS team at JPL for data processing and analysis support, especially Brian Knosp for data management and Ryan Fuller for development of the MLS L3 products. Thanks to the ACE team for providing ACE-FTS data, especially Chris Boone for the retrieval software and Patrick Sheese and Kaley Walker for making available the error flags and providing guidance on data quality and validation. Thanks to the GMAO for providing the MERRA-2 dataset, and to Brad Weir and Stephen Cohn for their roles in developing the M2-SCREAM reanalysis. Thanks to Lucien Froidevaux for helpful discussions. G.L. Manney was supported by the Jet Propulsion Laboratory (JPL) Microwave Limb Sounder team under JPL subcontract #1521127 to NWRA. K. Wargan was supported by NASA's Global Modeling and Assimilation core funding and by NASA's Modeling, Analysis and Prediction (MAP) grant "A new look at stratospheric chemistry with multispecies chemical data assimilation". Work at the Jet Propulsion Laboratory, California Institute of Technology, was carried out under a contract with the National Aeronautics and Space Administration (80NM0018D0004).

References

Abalos, M., Legras, B., & Shuckburgh, E. (2016). Interannual variability in effective diffusivity in the upper troposphere/lower stratosphere from reanalysis data. *Q. J. R. Meteorol. Soc.*, *142*(697), 1847–1861. doi: 10.1002/qj.2779

Albers, J. R., Perlwitz, J., Butler, A. H., Birner, T., Kiladis, G. N., Lawrence, Z. D., … Dias, J. (2018). Mechanisms governing interannual variability of stratosphere-to-troposphere ozone transport. *J. Geophys. Res.*, *123*(1), 234–260. Retrieved from `https://agupubs.onlinelibrary.wiley.com/doi/abs/10.1002/2017JD026890` doi: https://doi.org/10.1002/2017JD026890

Allen, D. R., & Nakamura, N. (2003). Tracer equivalent latitude: A diagnostic tool for isentropic transport studies. *J. Atmos. Sci.*, *60*, 287–304.

Baldwin, M. P., Gray, L. J., Dunkerton, T. J., Hamilton, K., Haynes, P. H., J, W., … Takahasi, M. (2001). The quasi-biennial oscillation. *Rev. Geophys.*, *39*, 179–229.

Bernath, P. F., et al. (2005). Atmospheric Chemistry Experiment (ACE): mission overview. *Geophys. Res. Lett.*, *32*. doi: 10.1029/2005GL022386

Bernhard, G. H., Fioletov, V. E., Grooß, J.-U., Ialongo, I., Johnsen, B., Lakkala, K., … Svendby, T. (2020). Record-breaking increases in Arctic solar ultraviolet radiation caused by exceptionally large ozone depletion in 2020. *Geophys. Res. Lett.*, *47*(24), e2020GL090844. Retrieved from `https://agupubs.onlinelibrary.wiley.com/doi/abs/10.1029/2020GL090844` (e2020GL090844 2020GL090844) doi: https://doi.org/10.1029/2020GL090844

Bloom, S. C., Takacs, L. L., da Silva, A. M., & Ledvina, D. (1996). Data assimilation using incremental analysis updates. *Mon. Weather Rev.*, *124*, 1256–1271.

Bognar, K., Alwarda, R., Strong, K., Chipperfield, M. P., Dhomse, S. S., Drummond, J. R., … Zhao, X. (2021). Unprecedented spring 2020 ozone depletion in the context of 20 years of measurements at Eureka, Canada. *J. Geophys. Res.*, *126*(8), e2020JD034365. Retrieved from `https://agupubs.onlinelibrary.wiley.com/doi/abs/10.1029/2020JD034365` (e2020JD034365 2020JD034365) doi: https://doi.org/10.1029/2020JD034365

Boone, C., Bernath, P., Cok, D., Jones, S., & Steffen, J. (2020). Version 4 retrievals for the atmospheric chemistry experiment Fourier transform spectrometer (ACE-FTS) and imagers. *Journal of Quantitative Spectroscopy and Radiative Transfer*, *247*, 106939. Retrieved from `https://www.sciencedirect.com/science/article/pii/S0022407319305916` doi: https://doi.org/10.1016/j.jqsrt.2020.106939

Butchart, N., & Remsberg, E. E. (1986). The area of the stratospheric polar vortex as a diagnostic for tracer transport on an isentropic surface. *J. Atmos. Sci.*, *43*, 1319–1339.

Butler, A. H., Lawrence, Z. D., Lee, S. H., Lillo, S. P., & Long, C. S. (2020). Differences between the 2018 and 2019 stratospheric polar vortex split events. *Quarterly Journal of the Royal Meteorological Society*, *146*(732), 3503-3521. Retrieved from `https://rmets.onlinelibrary.wiley.com/doi/abs/10.1002/qj.3858` doi: https://doi.org/10.1002/qj.3858

Curbelo, J., Chen, G., & Mechoso, C. R. (2021). Lagrangian analysis of the northern stratospheric polar vortex split in April 2020. *Geophys. Res. Lett.*, *48*(16), e2021GL093874. Retrieved from `https://agupubs.onlinelibrary.wiley.com/doi/abs/10.1029/2021GL093874` (e2021GL093874 2021GL093874) doi: https://doi.org/10.1029/2021GL093874

Domeisen, D. I., & Butler, A. H. (2020, December). Stratospheric drivers of extreme events at the Earth's surface. *Comm. Earth Environ.*, *1*(1), 59. Retrieved from `https://doi.org/10.1038/s43247-020-00060-z`

Dunkerton, T. J., & Delisi, D. P. (1986). Evolution of potential vorticity in the winter stratosphere of January-February 1979. *J. Geophys. Res.*, *91*, 1199–1208.

Feng, W., Dhomse, S. S., Arosio, C., Weber, M., Burrows, J. P., Santee, M. L., & Chipperfield, M. P. (2021). Arctic ozone depletion in 2019/20: Roles of chemistry, dynamics and the Montreal Protocol. *Geophys. Res. Lett.*, *48*(4), e2020GL091911. Retrieved from `https://agupubs.onlinelibrary.wiley.com/doi/abs/10.1029/2020GL091911` (e2020GL091911 2020GL091911) doi: https://doi.org/10.1029/2020GL091911

Fujiwara, M., Manney, G. L., Gray, L. J., & Wright, J. S. (Eds.). (2022). *SPARC Reanalysis Intercomparison Project (S-RIP) Final Report.* Retrieved from `https://www.sparc-climate.org/sparc-report-no-10/` (SPARC Report No. 10, WCRP-6/2021) doi: 10.17874/800dee57d13

Gelaro, R., McCarty, W., Suárez, M. J., Todling, R., Molod, A., Takacs, L., ... Zhao, B. (2017). The Modern-Era Retrospective Analysis for Research and Applications, Version-2 (MERRA-2). *J. Clim.*, *30*, 5419–5454. doi: doi:10.1175/JCLI-D-16-0758.1

Gille, J., Karol, S., Kinnison, D., Lamarque, J.-F., & Yudin, V. (2014). The role of midlatitude mixing barriers in creating the annual variation of total ozone in high northern latitudes. *J. Geophys. Res.*, *119*(15), 9578-9595. Retrieved from `https://agupubs.onlinelibrary.wiley.com/doi/abs/10.1002/2013JD021416` doi: 10.1002/2013JD021416

Global Modeling and Assimilation Office (GMAO). (2015). *MERRA-2 inst3_3d_asm_nv: 3d, 3-hourly,instantaneous, model-level, assimilation, assimilated meteorological fields v5.12.4, Greenbelt, MD, USA, Goddard Earth Sciences Data and Information Services Center (GES DISC), accessed 1 June 2022* [dataset]. doi: 10.5067/WWQSXQ8IVFW8

Global Modeling and Assimilation Office (GMAO). (2017). *Use of MERRA-2 for atmospheric chemistry and transport studies,.* Retrieved from `https://gmao.gsfc.nasa.gov/reanalysis/MERRA-2/docs/ANAvsASM.pdf`

Global Modeling and Assimilation Office (GMAO). (2022). *M2-SCREAM inst_3d_asm_met_chm_Nv: 3d, 3-hourly, instantaneous, pressure-level, assimilation, assimilated stratospheric chemistry fields, CoDAS, Icarus-3_2_p9, 0.5x0.625, Greenbelt, MD, USA, Goddard Earth Sciences Data and Information Services Center (GES DISC), accessed: [available by 1 July 2022]* [dataset]. doi: 10.5067/7PR3XRD6Q3NQ

Harvey, V. L., Randall, C. E., Goncharenko, L., Becker, E., & France, J. (2018). On the upward extension of the polar vortices into the mesosphere. *Journal of Geophysical Research: Atmospheres*, *123*(17), 9171–9191. Retrieved from `https://agupubs.onlinelibrary.wiley.com/doi/abs/10.1029/2018JD028815` doi: https://doi.org/10.1029/2018JD028815

Inness, A., Chabrillat, S., Flemming, J., Huijnen, V., Langenrock, B., Nicolas, J., ... Razinger, M. (2020). Exceptionally low Arctic stratospheric ozone in spring 2020 as seen in the CAMS reanalysis. *J. Geophys. Res.*, *125*(23), e2020JD033563. Retrieved from https://agupubs.onlinelibrary.wiley.com/doi/abs/10.1029/2020JD033563 (e2020JD033563 2020JD033563) doi: https://doi.org/10.1029/2020JD033563

Kidston, J., Scaife, A. A., Hardiman, S. C., Mitchell, D. M., Butchart, N., Baldwin, M. P., & Gray, L. J. (2015). Stratospheric influence on tropospheric jet streams, storm tracks and surface weather. *Nature Geoscience*, *8*. doi: http://dx.doi.org/10.1038/ngeo2424

Knudsen, B. M., & Grooß, J.-U. (2000). Northern midlatitude stratospheric ozone dilution in spring modeled with simulated mixing. *J. Geophys. Res.*, *105*, 6885–6890.

Lambert, A., Livesey, N., & Read, W. (2020). *MLS/Aura level 2 nitrous oxide (N2O) mixing ratio V005, Greenbelt, MD, USA, Goddard Earth Sciences Data and Information Services Center (GES DISC), accessed: [26 June 2022]* [dataset]. doi: https://doi.org/10.5067/Aura/MLS/DATA2515

Lambert, A., Livesey, N., Read, W., & Fuller, R. (2021a). *MLS/Aura level 3 daily binned nitrous oxide (N2O) mixing ratio on zonal and similar grids V005, Greenbelt, MD, USA, Goddard Earth Sciences Data and Information Services Center (GES DISC), accessed: [26 June 2022]* [dataset]. Retrieved from https://disc.gsfc.nasa.gov/datasets/ML3DZN2O_005/summary?keywords=mls doi: https://doi.org/10.5067/Aura/MLS/DATA/3116

Lambert, A., Livesey, N., Read, W., & Fuller, R. (2021b). *MLS/Aura level 3 daily binned water vapor (H2O) mixing ratio on zonal and similar grids V005, Greenbelt, MD, USA, Goddard Earth Sciences Data and Information Services Center (GES DISC), accessed: [26 June 2022]* [dataset]. Retrieved from https://disc.gsfc.nasa.gov/datasets/ML3DZH2O_005/summary?keywords=mls doi: https://doi.org/10.5067/Aura/MLS/DATA/3109

Lambert, A., Read, W., & Livesey, N. (2020). *MLS/Aura Level 2 water vapor (H2O) mixing ratio V005, Greenbelt, MD, USA, Goddard Earth Sciences Data and Information Services Center (GES DISC), accessed: [26 June 2022]* [dataset]. doi: https://doi.org/10.5067/Aura/MLS/DATA2508

Lawrence, Z. D., Manney, G. L., Minschwaner, K., Santee, M. L., & Lambert, A. (2015). Comparisons of polar processing diagnostics from 34 years of the ERA-Interim and MERRA reanalyses. *Atmos. Chem. Phys.*, *15*, 3873–3892.

Lawrence, Z. D., Perlwitz, J., Butler, A. H., Manney, G. L., Newman, P. A., Lee, S. H., & Nash, E. R. (2020). The remarkably strong Arctic stratospheric polar vortex of winter 2020: Links to record-breaking Arctic oscillation and ozone loss. *J. Geophys. Res.*, *125*(22), e2020JD033271. Retrieved from https://agupubs.onlinelibrary.wiley.com/doi/abs/10.1029/2020JD033271 (e2020JD033271 10.1029/2020JD033271) doi: https://doi.org/10.1029/2020JD033271

Lee, J. N., Wu, D. L., Manney, G. L., & Schwartz, M. J. (2009). Aura Microwave Limb Sounder observations of the northern annular mode: From the mesosphere to the upper troposphere. *Geophys. Res. Lett.*, *36*(20). Retrieved from https://agupubs.onlinelibrary.wiley.com/doi/abs/10.1029/2009GL040678 doi: 10.1029/2009GL040678

Lee, J. N., Wu, D. L., Manney, G. L., Schwartz, M. J., Lambert, A., Livesey, N. J., … Read, W. G. (2011). Aura Microwave Limb Sounder observations of the polar middle atmosphere: Dynamics and transport of CO and H_2O. *J. Geophys. Res.*, *116*. doi: 10.1029/2010JD014608

Livesey, N. J., Read, W. G., Froidevaux, L., Lambert, A., Santee, M. L., Schwartz, M. J., … Nedoluha, G. E. (2021). Investigation and amelioration of long-term instrumental drifts in water vapor and nitrous oxide measurements from the Aura Microwave Limb Sounder (MLS) and their implications for studies of variability and trends. *Atmos. Chem. Phys.*, *21*(20), 15409–15430. Retrieved from https://acp.copernicus.org/articles/21/15409/2021/ doi: 10.5194/acp-21-15409-2021

Livesey, N. J., Read, W. G., Wagner, P. A., Froidevaux, L., Lambert, A., Manney, G. L., . . . Lay, R. R. (2018). *EOS MLS version 4.2x level 2 data quality and description document* (Tech. Rep.). JPL. (Available from http://mls.jpl.nasa.gov/)

Livesey, N. J., Read, W. G., Wagner, P. A., Froidevaux, L., Lambert, A., Manney, G. L., . . . Lay, R. R. (2020). *EOS MLS version 4.2x level 2 and 3 data quality and description document* (Tech. Rep.). JPL. (Available from http://mls.jpl.nasa.gov/)

Lukianova, R., Kozlovsky, A., & Lester, M. (2021). Upper stratosphere-mesosphere-lower thermosphere perturbations during the formation of the Arctic polar night jet in 2019–2020. *Geophys. Res. Lett.*, *48*(19), e2021GL094926. Retrieved from `https://agupubs.onlinelibrary.wiley.com/doi/abs/10.1029/2021GL094926` (e2021GL094926 2021GL094926) doi: https://doi.org/10.1029/2021GL094926

Ma, Z., Gong, Y., Zhang, S., Zhou, Q., Huang, C., Huang, K., & Li, G. (2022). First observational evidence for the role of polar vortex strength in modulating the activity of planetary waves in the MLT region. *Geophys. Res. Lett.*, *49*(3), e2021GL096548. Retrieved from `https://agupubs.onlinelibrary.wiley.com/doi/abs/10.1029/2021GL096548` (e2021GL096548 2021GL096548) doi: https://doi.org/10.1029/2021GL096548

Manney, G. L., Daffer, W. H., Zawodny, J. M., Bernath, P. F., Hoppel, K. W., Walker, K. A., . . . Waters, J. W. (2007). Solar occultation satellite data and derived meteorological products: Sampling issues and comparisons with aura microwave limb sounder. *J. Geophys. Res.*, *112*(D24S50). doi: 10.1029/2007JD008709

Manney, G. L., Harwood, R. S., MacKenzie, I. A., Minschwaner, K., Allen, D. R., Santee, M. L., . . . Fuller, R. A. (2009). Satellite observations and modelling of transport in the upper troposphere through the lower mesosphere during the 2006 major stratospheric sudden warming. *Atmos. Chem. Phys.*, *9*, 4775–4795.

Manney, G. L., Hegglin, M. I., Daffer, W. H., Santee, M. L., Ray, E. A., Pawson, S., . . . Walker, K. A. (2011). Jet characterization in the upper troposphere/lower stratosphere (UTLS): Applications to climatology and transport studies. *Atmos. Chem. Phys.*, *11*, 6115–6137.

Manney, G. L., & Lawrence, Z. D. (2016). The major stratospheric final warming in 2016: dispersal of vortex air and termination of Arctic chemical ozone loss. *Atmos. Chem. Phys.*, *16*(23), 15371–15396. Retrieved from `https://www.atmos-chem-phys.net/16/15371/2016/` doi: 10.5194/acp-16-15371-2016

Manney, G. L., Lawrence, Z. D., Santee, M. L., Livesey, N. J., Lambert, A., & Pitts, M. C. (2015). Polar processing in a split vortex: Arctic ozone loss in early winter 2012/2013. *Atmos. Chem. Phys.*, *15*, 4973–5029.

Manney, G. L., Lawrence, Z. D., Santee, M. L., Read, W. G., Livesey, N. J., Lambert, A., . . . Schwartz, M. J. (2015). A minor sudden stratospheric warming with a major impact: Transport and polar processing in the 2014/2015 arctic winter. *Geophys. Res. Lett.*, *42*, 7808–7816. doi: 10.1002/2015GL065864

Manney, G. L., Livesey, N. J., Santee, M. L., Froidevaux, L., Lambert, A., Lawrence, Z. D., . . . Fuller, R. A. (2020). Record-low Arctic stratospheric ozone in 2020: MLS observations of chemical processes and comparisons with previous extreme winters. *Geophys. Res. Lett.*, *47*(16), e2020GL089063. Retrieved from `https://agupubs.onlinelibrary.wiley.com/doi/abs/10.1029/2020GL089063` (e2020GL089063 10.1029/2020GL089063) doi: https://doi.org/10.1029/2020GL089063

Manney, G. L., Santee, M. L., Rex, M., Livesey, N. J., Pitts, M. C., Veefkind, P., . . . Zinoviev, N. S. (2011). Unprecedented Arctic ozone loss in 2011. *Nature*, *478*, 469–475.

Manney, G. L., Schwartz, M. J., Krüger, K., Santee, M. L., Pawson, S., Lee, J. N., . . . Livesey, N. J. (2009). Aura Microwave Limb Sounder observations of dynamics and transport during the record-breaking 2009 Arctic stratospheric major warming. *Geophys. Res. Lett.*, *36*. doi: 10.1029/2009GL038586

Manney, G. L., Zurek, R. W., O'Neill, A., & Swinbank, R. (1994). On the motion of air through the stratospheric polar vortex. *J. Atmos. Sci.*, *51*, 2973–2994.

Marchand, M., Godin, S., Hauchecorne, A., Lefevre, R., & Chipperfield, M. (2003). Influence of polar ozone loss on northern midlatitude regions estimated by a high-resolution chemistry transport model during winter 1999/2000. *J. Geophys. Res.*, *108*, 8326. doi: 10.1029/2001JD000906

McDonald, A. J., & Smith, M. (2013). A technique to identify vortex air using carbon monoxide observations. *J. Geophys. Res.*, *118*, 12,719–12,733. doi: 10.1002/2012JD019257

Nakamura, N. (1996). Two-dimensional mixing, edge formation, and permeability diagnosed in area coordinates. *J. Atmos. Sci.*, *53*, 1524–1537.

Rupp, P., Loeffel, S., Garny, H., Chen, X., Pinto, J. G., & Birner, T. (2022). Potential links between tropospheric and stratospheric circulation extremes during early 2020. *J. Geophys. Res.*, *127*(3), e2021JD035667. Retrieved from `https://agupubs.onlinelibrary.wiley.com/doi/abs/10.1029/2021JD035667` (e2021JD035667 2021JD035667) doi: https://doi.org/10.1029/2021JD035667

Santee, M. L., MacKenzie, I. A., Manney, G. L., Chipperfield, M. P., Bernath, P. F., Walker, K. A., ... Waters, J. W. (2008). A study of stratospheric chlorine partitioning based on new satellite measurements and modeling. *J. Geophys. Res.*, *113*. doi: 10.1029/2007JD009057

Schwartz, M., Froidevaux, L., Livesey, N., & Read, W. (2020). *MLS/Aura level 2 ozone (O3) mixing ratio V005, Greenbelt, MD, USA, Goddard Earth Sciences Data and Information Services Center (GES DISC), accessed: [26 june 2022]* [dataset]. doi: https://doi.org/10.5067/Aura/MLS/DATA2506

Schwartz, M., Froidevaux, L., Livesey, N., Read, W., & Fuller, R. (2021). *MLS/Aura level 3 daily binned ozone (O3) mixing ratio on zonal and similar grids V005, Greenbelt, MD, USA, Goddard Earth Sciences Data and Information Services Center (GES DISC), accessed: [26 June 2022]* [dataset]. Retrieved from `https://disc.gsfc.nasa.gov/datasets/ML3DZO3_005/summary?keywords=mls` doi: https://doi.org/10.5067/Aura/MLS/DATA/3105

Schwartz, M., Pumphrey, H., Livesey, N., & Read, W. (2020). *MLS/Aura level 2 carbon monoxide (CO) mixing ratio V005, Greenbelt, MD, USA, Goddard Earth Sciences Data and Information Services Center (GES DISC), accessed: [26 June 2022]* [dataset]. doi: https://doi.org/10.5067/Aura/MLS/DATA2506

Schwartz, M., Pumphrey, H., Livesey, N., Read, W., & Fuller, R. (2021). *MLS/Aura level 3 daily binned carbon monoxide (CO) mixing ratio on zonal and similar grids V005, Greenbelt, MD, USA, Goddard Earth Sciences Data and Information Services Center (GES DISC), accessed: [26 June 2022]* [dataset]. Retrieved from `https://disc.gsfc.nasa.gov/datasets/ML3DZCO_005/summary?keywords=mls` doi: https://doi.org/10.5067/Aura/MLS/DATA/3105

Sheese, P., & Walker, K. (2020). *Data Quality Flags for ACE-FTS Level 2 Version 4.1 Data Set.* Scholars Portal Dataverse. Retrieved from `https://doi.org/10.5683/SP2/BC4ATC` doi: 10.5683/SP2/BC4ATC

Sheese, P. E., Boone, C. D., & Walker, K. A. (2015). Detecting physically unrealistic outliers in ACE-FTS atmospheric measurements. *Atmospheric Measurement Techniques*, *8*(2), 741–750. Retrieved from `https://amt.copernicus.org/articles/8/741/2015/` doi: 10.5194/amt-8-741-2015

Tao, M., Konopka, P., Ploeger, F., Grooß, J.-U., Müller, R., Volk, C. M., ... Riese, M. (2015). Impact of the 2009 major sudden stratospheric warming on the composition of the stratosphere. *Atmospheric Chemistry and Physics*, *15*(15), 8695–8715. Retrieved from `https://acp.copernicus.org/articles/15/8695/2015/` doi: 10.5194/acp-15-8695-2015

Wargan, K., Weir, B., Manney, G. L., Cohn, S. E., Knowland, K. E., Wales, P., & Livesey, N. J. (2022). *M2-SCREAM: A stratospheric composition reanalysis of Aura MLS data with MERRA-2 transport.* (submitted to *Earth Systems Science Datasets*)

Wargan, K., Weir, B., Manney, G. L., Cohn, S. E., & Livesey, N. J. (2020). The anomalous 2019 Antarctic ozone hole in the GEOS constituent data assimilation system with MLS observations. *Journal of Geophysical Research: Atmospheres*, *125*(18), e2020JD033335. Retrieved from `https://agupubs.onlinelibrary.wiley.com/doi/abs/10.1029/2020JD033335` (e2020JD033335 2020JD033335) doi: https://doi.org/10.1029/2020JD033335

Waters, J. W., Froidevaux, L., Harwood, R. S., Pickett, R. F. J. H. M., Read, W. G., Siegel, P. H., ... Walch, M. J. (2006). The Earth Observing System Microwave Limb Sounder (EOS MLS) on the Aura satellite. *IEEE Trans. Geosci. Remote Sens.*, *44*, 1075–1092.

Weber, M., Arosio, C., Feng, W., Dhomse, S. S., Chipperfield, M. P., Meier, A., ... Rozanov, A. (2021). The unusual stratospheric Arctic winter 2019/20: Chemical ozone loss from satellite observations and TOMCAT chemical transport model. *J. Geophys. Res.*, *126*(6), e2020JD034386. Retrieved from `https://agupubs.onlinelibrary.wiley.com/doi/abs/10.1029/2020JD034386` (e2020JD034386 2020JD034386) doi: https://doi.org/10.1029/2020JD034386

Wohltmann, I., von der Gathen, P., Lehmann, R., Deckelmann, H., Manney, G. L., Davies, J., ... Rex, M. (2021). Chemical evolution of the exceptional Arctic stratospheric winter 2019/2020 compared to previous Arctic and Antarctic winters. *J. Geophys. Res.*, *126*(18), e2020JD034356. Retrieved from `https://agupubs.onlinelibrary.wiley.com/doi/abs/10.1029/2020JD034356` (e2020JD034356 2020JD034356) doi: https://doi.org/10.1029/2020JD034356

Wohltmann, I., von der Gathen, P., Lehmann, R., Maturilli, M., Deckelmann, H., Manney, G. L., ... Rex, M. (2020). Near-complete local reduction of Arctic stratospheric ozone by severe chemical loss in spring 2020. *Geophys. Res. Lett.*, *47*(20), e2020GL089547. Retrieved from `https://agupubs.onlinelibrary.wiley.com/doi/abs/10.1029/2020GL089547` (e2020GL089547 10.1029/2020GL089547) doi: https://doi.org/10.1029/2020GL089547